SURFACE-COVERAGE ALGORITHMS FOR FILAMENT WINDING OF NON-AXISYMMETRIC CYLINDRICAL PARTS

J.M. Dolan, P.K. Khosla, and S.N. Talukdar
Carnegie Mellon University, Pittsburgh, PA[1]

ABSTRACT

Filament winding of fiber-reinforced composites requires precise control of the filament band path on the mandrel surface onto which it is wound. In helical filament winding, a basic path is selected for traversing the mandrel once. This path is then shifted an appropriate number of times in order to obtain a closed or near-closed filament layer. The current paper corrects a flaw in previous presentations [1, 2, 3] of an axisymmetric closure algorithm. Closure algorithms and examples of their implementation are also presented for smooth and polygonal non-axisymmetric parts of constant cross-section ("cylinders"). These algorithms can be used to wind non-axisymmetric cylindrical parts on standard two-degree-of-freedom winding machines.

KEY WORDS: Filament Winding, Automation, Software

1.0 INTRODUCTION

During helical filament winding, filament is typically wound onto the surface of a rotating mandrel by a filament delivery point which moves laterally back and forth along the length of the mandrel. Unlike axisymmetric parts, non-axisymmetric filament-wound parts have received relatively little attention in the literature. Several papers describe CAD/CAM systems for the determination of control winding data for non-axisymmetric parts [4, 5, 6, 7, 8], but give little detail on the mathematics of delivery point motion or surface coverage. Allard et al. [9], in a treatment of elliptical shapes, also do not present the mathematics underlying non-axisymmetric winding, stating that the situation is complex and is not generally amenable to closed-form analytical solution.

In order to helically wind complex part geometries, two basic tasks must be carried out. First, the desired path of the filament band on the surface of the mandrel must be specified. Second, a mathematical description of the coordinated motions of the machine axes needed to achieve the desired path must be given, i.e., the "control data" must be determined. The first task includes single-circuit specification and surface coverage. Single-circuit specification gives the filament path to be followed for a single traversal of the mandrel. Surface coverage involves ensuring that successive circuits are shifted appropriately with respect to one another about the mandrel circumference so that the final winding just covers the mandrel surface, or has an acceptable degree of gapping or overlapping between adjacent circuits.

Using a "geometric approach," Mazumdar and Hoa [10, 11] present partial solutions to the above-mentioned problems of path specification and axis coordination for non-axisymmetric cylindrical (i.e., constant-cross-section) mandrels. In particular, they solve the axis-coordination problem for a constant-winding-angle path for a half-circuit for both smooth and polygonal mandrel shapes. They do not, however, address the surface-coverage problem. In addition, for the flat mandrel ends occurring in the case of a cylindrical mandrel, the necessity for the filament to turn around in the end regions requires a path with non-constant winding angle. In this paper, previous

1. We gratefully acknowledge the generous support of ABB TRAFO-BB GmbH, Brilon, Germany, in performing this work.

work is extended to include arbitrary path specification and surface coverage for both smooth and polygonal non-axisymmetric shapes.

2.0 PROBLEM FORMULATION AND SOLUTION

2.1 Smooth Shapes

2.1.1 Geometry

The following treatment summarizes that given by Mazumdar and Hoa [10]. Fig. 1 shows a mandrel cross-section with a smooth (i.e., differentiable) contour. The y-axis is inscribed on the mandrel and makes an angle θ with the fixed axis Y as the mandrel rotates counterclockwise about its longitudinal axis of rotation A. The fiber CD originates at the delivery point D and is tangent to the mandrel at the point C, the contact or winding point. Its length l perpendicular to axis A varies depending on the point of contact. The variable d designates the distance of the delivery point perpendicular to axis A, and λ represents its (constant) angle of elevation from the Y-axis. The angle between segments CD and AD is α.

The mandrel's cross-sectional profile is specified as

$$r = F(\phi) \qquad \text{(EQ 1)}$$

where r is the radius at an angle ϕ measured from the inscribed axis y. The angle ν is defined as that between the normal to the mandrel profile at C and the extension of the radius there.

The following relationships result [10]:

$$\nu = \text{atan2}\left(-\frac{dr}{d\phi}, r\right) \qquad \text{(EQ 2)}$$

$$\sin\alpha = \frac{r\cos\nu}{d} \qquad \text{(EQ 3)}$$

$$l = d\cos\alpha - r\sin\nu \qquad \text{(EQ 4)}$$

$$\theta = \frac{\pi}{2} - \alpha - \phi - \nu + \lambda \qquad \text{(EQ 5)}$$

Given a value for ϕ, which uniquely specifies a point on the mandrel perimeter, Equations (1)-(5) may be solved successively to obtain values for r, ν, α, l, and θ, respectively.

2.1.2 Equation of Motion

From Fig. 2, the tangent of the instantaneous winding angle, θ_f, can be written as both a ratio of velocities and a ratio of distances:

$$\tan\theta_f = \frac{v_x}{v_l} = \frac{X - x}{l} \qquad \text{(EQ 6)}$$

where v_x and v_l are the longitudinal and lateral velocities of the winding point C with respect to the surface of the mandrel, and X and x are the longitudinal positions of the delivery point D and winding point C, respectively. From (6), we obtain the winding equation of motion

$$v_x \equiv \frac{dx}{dt} = \frac{v_l}{l}(X - x) \qquad \text{(EQ 7)}$$

FIGURE 1. Mandrel and fiber position at mandrel rotation angle θ

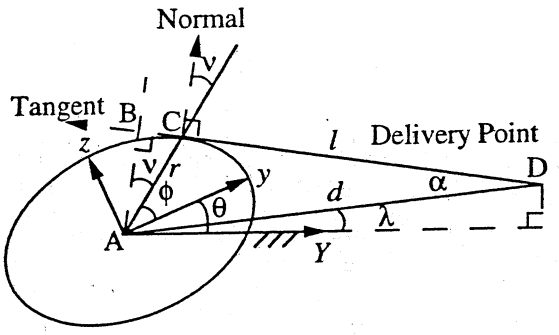

FIGURE 2. Delivery Point Geometry

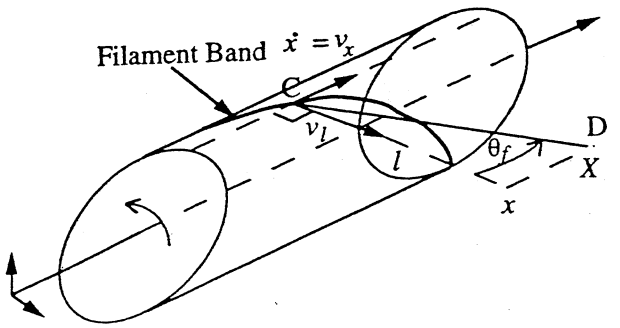

For complex shapes, it is computationally inconvenient to integrate (7) in the time domain. It is preferable to multiply through by the differential dt, noting that the expression $v_l\,dt$ is the differential arc length, ds, moved laterally along the perimeter of the mandrel in time dt. Thus,

$$ds \equiv v_l dt = \left(-\sqrt{r^2 + \left(\frac{dr}{d\phi}\right)^2}\right) d\phi \qquad \text{(EQ 8)}$$

where the last expression is the differential arc length in polar coordinates. The negative sign arises from the fact that ds and $d\phi$ have opposite signs.

Equation (7) can now be rewritten

$$\frac{dx}{ds} = \frac{X - x}{l} \qquad \text{(EQ 9)}$$

or, alternatively,

$$\frac{dx}{d\phi} = \frac{-G(\phi)}{l(\phi)}(X - x) \qquad \text{(EQ 10)}$$

where

$$G(\phi) \equiv \sqrt{r^2 + \left(\frac{dr}{d\phi}\right)^2} \qquad \text{(EQ 11)}$$

The integration of (10) may now be performed numerically with ϕ as the independent variable. The θ-value corresponding to a given ϕ-value may be found from Equations (1)-(5).

2.1.3 Winding-Angle Control

A solution for the delivery point $X(\phi)$ is sought which achieves a desired winding-angle trajectory. In the most general case, the winding angle varies over the length of the mandrel, especially during turnaround in the mandrel end-regions. Both sides of the equation of motion (9) are equal to the tangent of the winding angle at any given point on the mandrel. Thus,

$$dx = (\tan\theta_f)\, ds \qquad \text{(EQ 12)}$$

$$X = x + l\tan\theta_f \qquad \text{(EQ 13)}$$

The winding-angle variation can be conveniently expressed as a function of the winding-point perimeter position s. A numerical solution for $X(\phi)$ is derived in iterative form from (12) and (13) as follows. The integral of (12) between ϕ_{i-1} and ϕ_i is estimated assuming a small ϕ-increment:

$$x_i = x_{i-1} + (\Delta s_{i-1,i})\tan\theta_f(s_i) \qquad \text{(EQ 14)}$$

where

$$\Delta s_{i-1,i} \approx \int_{\phi_{i-1}}^{\phi_i} ds$$

approximates the arc length between the mandrel perimeter points corresponding to ϕ_{i-1} and ϕ_i. Equation (13) is then written using subscripts to denote evaluation at ϕ_i

$$X_i = x_i + l_i\tan\theta_f(s_i) \qquad \text{(EQ 15)}$$

The length $\Delta s_{i-1,i}$ may be approximated either by estimating the arc-length integral

$$\Delta s_{i-1,i} \equiv -\frac{1}{2}(\phi_i - \phi_{i-1})\,(G_i + G_{i-1}) \qquad \text{(EQ 16)}$$

or by finding the straight-line distance between the mandrel perimeter points, as is done in [10]:

$$\Delta s_{i-1,i} \equiv \sqrt{(y_i - y_{i-1})^2 + (z_i - z_{i-1})^2} \qquad \text{(EQ 17)}$$

$$y_i = r_i\cos\phi_i \qquad z_i = r_i\sin\phi_i$$

In cases where the mandrel profile $r(\phi)$ is given as a set of discrete pairs (r_i, ϕ_i), rather than as a differentiable function, the second method must be used, since G involves the first derivative of $r(\phi)$. The first method permits an arbitrary degree of accuracy, whereas the second method is computationally more efficient.

The iteration given by (14) and (15) provides a set of discrete pairs (X_i, ϕ_i) giving the relationship between the angle ϕ and the filament support position X in order to achieve a desired, potentially varying, winding angle. The values x_0 and ϕ_0 must be specified to initialize the iteration. If the winding angle θ_f is made constant, (14) and (15) are identical to the iteration presented in [10]. This section has modified these equations to provide for a non-constant winding angle, and has shown the relationship between these discrete equations and the continuous differential winding equation.

2.1.4 *Surface-Coverage Algorithm*

A pass is defined as a single back-and-forth traversal of the delivery point along the mandrel length, from the "start" end of the mandrel to the "far" end and back (see Fig. 3). A helically wound filament layer is laid down by executing a sufficient number of passes to cover the mandrel. A single layer defined in this way involves a double thickness of filament, with one set of bands laid down in each direction. The winding-angle control algorithm presented in [10] gives the filament support trajectory for a single pass, but does not address the problem of surface coverage. There are three steps in ensuring surface coverage. First, given the mandrel profile, desired winding angle, and filament band width, the number of passes required for closure must be determined. Second, the positions of the band centers about the mandrel profile at the start and far ends must be determined. Third, the delivery point pauses needed at the mandrel endpoints in order to properly space the bands must be determined.

FIGURE 3. Mandrel-End Arrival and Departure Angles

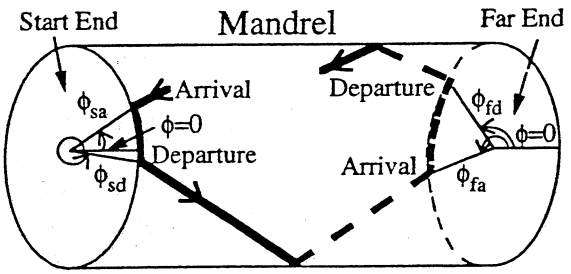

Number of Bands m. The total mandrel perimeter P is given by

$$P = \int_0^P dp = \int_0^{2\pi} G(\phi)\,d\phi \qquad \text{(EQ 18)}$$

where $G(\phi)$ is defined in (11).

Given winding angle θ_f and filament band width B, the band width in the direction of the mandrel perimeter is

$$B_p = \frac{B}{\tan\theta_f} \qquad \text{(EQ 19)}$$

The number of bands required for surface coverage is given by the perimeter divided by the band width in the direction of the perimeter

$$m = \frac{P}{B_p} = \frac{P\tan\theta_f}{B} \qquad \text{(EQ 20)}$$

The number of bands must be an integer for proper closure, so the value found in (20) should be rounded to the nearest integer and then re-inserted into (20) to find an adjusted winding angle θ_f.

Band-Center Positions ϕ_{ci}. The initial band-center position ϕ_{c0} on the mandrel perimeter at the start end is arbitrary. Once it is specified, the other band-center positions ϕ_{ci} should be spaced at equal distances B_p along the mandrel perimeter. This is achieved for the start end by calculating the following integral

$$i \times B_p = \int_{\phi_{c0}}^{\phi_{ci}} G(\phi)\,d\phi \qquad \text{(EQ 21)}$$

for $i = 0, 1, \ldots, m\text{-}1$, where the unknown is the upper limit of integration. For simplicity, the same set of band-center positions may be used for the far end.

Pause Values ϕ_p. For a given pass, the filament arrives at the start end at an angular position ϕ_{sa} and departs at position ϕ_{sd} (see Fig. 3). Similarly, the band arrives and departs at the far end at angular positions ϕ_{fa} and ϕ_{fd}, respectively. The difference between the arrival and departure angles at a given end is the pause value for that end for the current pass. Pause values must be chosen so that the departure angles correspond to the band-center positions determined in (21). Because the pause values vary from pass to pass in the general case, a schedule of pause values for each pass and each end must be calculated. The schedule of pause values may be determined as follows:

1. Identify the arrival angle at the start end as ϕ_{sa}. For the initial pass, $\phi_{sa} = \phi_{c0}$. The longitudinal positions of the winding point at the start and far ends are x_s and x_f, respectively.
2. Pause at the start end until the band contact point corresponds to the first available of the ϕ_{ci} found in (21). The contact angle at the end of the pause is the start-end depar-

ture angle ϕ_{sd}. The start-end pause value is $\phi_{sp} = \phi_{sa} - \phi_{sd}$, i.e., the difference between the arrival and departure angles.

3. Solve for the arrival angle at the far end of the mandrel, ϕ_{fa}, by performing the iteration (14)-(15) with $x_0 = x_s$, $\phi_0 = \phi_{sd}$, until x_i is equal to x_f.
4. As at the start end, pause until the band contact point corresponds to the first available of the ϕ_{ci}. The resulting far-end departure angle is ϕ_{fd}. The far-end pause value is $\phi_{fp} = \phi_{fa} - \phi_{fd}$, i.e., the difference between the arrival and departure angles.
5. Solve for the start-end arrival angle for the next pass, ϕ_{sa}, by performing the iteration (14)-(15) with $x_0 = x_f$, $\phi_0 = \phi_{fd}$, until x_i is equal to x_s.
6. Perform steps 1 through 5 a total of m times, using the angle ϕ_{sa} found in step 5 each time as the new start-end arrival angle in step 1. Once all m positions have been filled at both ends, the layer is complete.

Circular Cylinders

Flawed surface-coverage algorithms for circular cylinders were presented in [1], [2], and [3]. The correct algorithm is presented here. In the case of a circular mandrel profile, $G(\phi) = r$, a constant. The rotational symmetry of the circle permits a single pause value, since the shift along the perimeter is the same for each pass, irrespective of the starting-point on the mandrel perimeter. The number of bands is calculated as in (20), with the perimeter P given by $2\pi r$. The band centers are at the evenly spaced positions $BC_i = \frac{i}{m}$, $i = 0, 1, \ldots, m\text{-}1$, using units of mandrel turns, rather than radians. The change in ϕ (i.e., the shift of the filament contact point along the mandrel perimeter) from one pass to the next without pause at any given cross-section is now constant:

$$n_\phi = \frac{2L}{\pi D \tan\theta_f} \qquad \text{(EQ 22)}$$

where D is the diameter of the circle. In the absence of pauses at the mandrel endpoints, the fractional part of n_ϕ is the shift at a given cross-section, in fractions of a turn, between band center positions in successive passes. Thus, for example, if $n_\phi = 2.25$, two successive band centers at a given cross-section will be separated by $0.25 = \frac{1}{4}$ turn, or 90 degrees.

The surface-coverage algorithm must now choose a pause value n_ψ such that the total number of mandrel turns per pass $n = n_\phi + n_\psi$, which is also the total shift in turns between bands at a given cross-section, results in all m bands being laid down at the distinct positions BC_i. The algorithm presented in [2] and [3] puts the following condition on n:

$$M = \frac{k \pm \frac{1}{m}}{n} \qquad \text{(EQ 23)}$$

where k is some positive integer, and the pattern number, M, must be equal to a positive integer. The pattern number M is the number of passes necessary to arrive at a band center adjacent to the initial one. However, satisfaction of (23), although necessary, is not a sufficient condition to produce a valid solution for n. This can be seen by considering a simple example. If $m = 24$ and $M = 3$, the solution

$$n = 1\frac{8\frac{1}{3}}{24}$$

satisfies (23) with $k = 4$, since

$$Mn = 3n = 4\frac{1}{24}$$

indicating that the band-center position after three passes is adjacent to the initial position. However, the band-center positions after the first and second passes are

$$\frac{8\frac{1}{3}}{24} \text{ and } \frac{16\frac{2}{3}}{24},$$

respectively, and are not integer multiples of $\frac{1}{24}$. Incorrect solutions of this type result in gapping or overlapping between groups of bands.

The correct condition to place on n is that its fractional part, n_f, be equal to an integer multiple of $\frac{1}{m}$:

$$n_f = \frac{j}{m} \qquad \text{(EQ 24)}$$

where j is an integer, $0 < j < m$. In order for all the band-center positions to be filled, j and m must be relatively prime, i.e., j and m must have no common factor greater than 1.

In summary, solutions for the circular case are found as follows:

1. Find the per-pass band-center position shift

$$n_\phi = \frac{2L}{\pi D \tan\theta_f} \qquad \text{(EQ 25)}$$

2. Find the set of integer multiples $\{j_s\}$ of $\frac{1}{m}$ which produce the fractional parts, n_f, of valid solutions for the number of mandrel turns per pass, n. The j_s consist of all j, $0 < j < m$, such that j and m are relatively prime, i.e., they have no common factor greater than 1.

3. Find valid solutions $n \geq n_\phi$ having allowable fractional parts

$$\{n_f\} = \frac{\{j_s\}}{m} \qquad \text{(EQ 26)}$$

The pause value corresponding to a given solution for n is $n_\psi = n - n_\phi$.

4. If desired, find the pattern number M for a particular multiple j_s from

$$M = \frac{(k \times m) \pm 1}{j_s} \qquad \text{(EQ 27)}$$

where the integer k is incremented starting with 1 until M equals an integer. Alternatively, the band-center position sequence can be generated and inspected to determine M.

2.1.5 Surface-Coverage Example

To illustrate the smooth-shape closure algorithm, we choose an ellipsoidal mandrel with length L = 1000 *mm* and ellipse semi-major axes a = 220 *mm* and b = 110 *mm*. The elliptic mandrel cross-section is given in Cartesian coordinates by

$$\frac{y^2}{a^2} + \frac{z^2}{b^2} = 1 \qquad \text{(EQ 28)}$$

As in [10], the perimeter is divided into 1440 linear segments according to (17), using a 0.25-degree ϕ-interval. Substituting $y = r\cos\phi$ and $z = r\sin\phi$ into (28) yields

$$r = F(\phi) = \frac{ab}{\sqrt{b^2\cos^2\phi + a^2\sin^2\phi}} \qquad \text{(EQ 29)}$$

corresponding to (1). Differentiation of (29) yields

$$\frac{dr}{d\phi} = \frac{ab\,(b^2 - a^2)\sin 2\phi}{2\,(b^2\cos^2\phi + a^2\sin^2\phi)^{3/2}} \qquad \text{(EQ 30)}$$

With a filament band width B = 42 *mm* and a desired winding angle θ_f = 30°, the integer number of bands m = 15 is found from (19) and (20) after calculating the ellipse perimeter P = 1065.7 *mm* from (18). Re-insertion of m into (20) leads to an adjusted winding angle θ_f = 30.59°.

The band-center positions ϕ_{ci} in degrees are now found from (21) to be {0.0, 17.7, 36.7, 63.5, 99.2, 131.2, 153.3, 170.9, 189.0, 206.7, 228.8, 260.8, 296.5, 323.3, 342.3}. For simplicity, these band-center positions are used at both ends of the mandrel. In order to begin the winding at band-center position ϕ_{c0}, the delivery point is positioned at an elevation above the axis of rotation equal to the ellipse major axis a. The distance d of the delivery point from the axis of rotation,, must be greater than the semi-major axis a in order to avoid collisions. The distance $d = a + 130 = 350$ *mm* is chosen, giving an elevation angle

$$\lambda = \text{asin}\left(\frac{a}{d}\right) = 38.9°$$

FIGURE 4. Band-Center Trajectory Specification

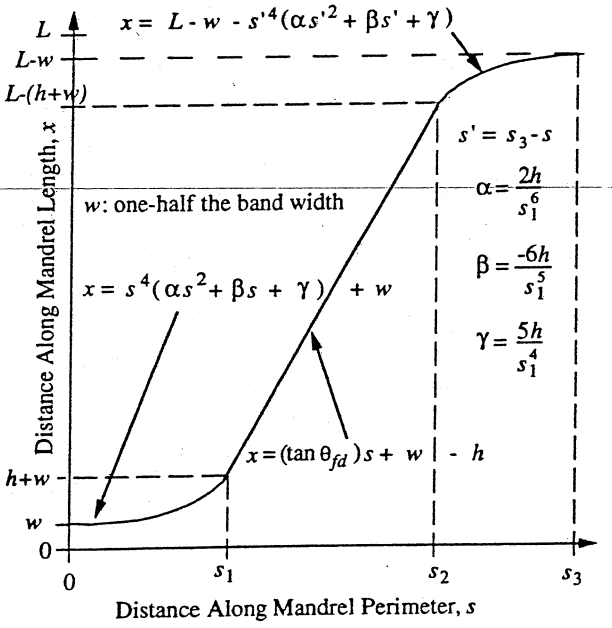

A suitable filament-band trajectory $x(s)$ must now be specified. Fig. 4 shows one such band trajectory. Two end-region polynomial sections are linked by a constant-winding-angle section in the middle region. The winding angle thus starts at 0°, ramps up to the desired value θ_{fd}, and ramps down to 0° at the other end, allowing for the necessary reversal of the filament support direction at the mandrel end-

points. The desired size of the end regions is specified by the constant h. The inset w at either end of the mandrel is equal to half the band width. If the band is to remain on the mandrel, the contact point c of the band center may not exceed the limits $w \le c \le L - w$. The order and coefficients of the polynomial are chosen to ensure continuity of the third derivative of x with respect to s at the junctures of the different portions of the curve, which in turn ensures a smoothly varying delivery point velocity. In practice, the filament-band trajectory would need to additionally take into account the conditions of frictional equilibrium of the band in the non-geodesically wound mandrel end regions in order to prevent slippage from occuring [12].

Using this band-center trajectory specification, we can write the tangent of the actual winding angle as a function of the perimeter distance s

$$t_i = \tan\theta_f(s) \qquad s_{i-1} \le s \le s_i$$

$$t_1 = \left(\frac{2hs^3}{s_1^6}\right)(6s^2 - 15s_1 s + 10s_1^2)$$

$$t_2 = \tan\theta_{fd}$$

$$t_3 = \left(\frac{2hs'^2}{s_1^6}\right)(6s'^2 - 15s_1 s' + 10s_1 s')$$

$$s' \equiv s_3 - s$$

where θ_{fd} is the desired, or nominal, winding angle, $\theta_f(s)$ is the actual winding angle for a given value of s, and

$$s_0 = 0 \qquad s_1 = \frac{2h}{\tan\theta_{fd}}$$

$$s_2 = \frac{L-2w}{\tan\theta_{fd}} \qquad s_3 = \frac{L+2(h-w)}{\tan\theta_{fd}}$$

The initial perimeter position for a given pass is taken as $s = 0$.

The delivery point trajectories and pause values are now calculated by using the function $\tan\theta_f(s)$ in (14) and (15) with an end-region size h = 80 *mm*. Table 1 gives a schedule of θ-values for the current example in units of mandrel "turns" (# turns = $\frac{\theta}{360°}$). "Travel turns" refers to the number of rotations number, BC for the band-center position occupied on a given half-pass. Unlike the circular case, in which the pause and travel values remain constant, the pause value varies between 0.0 and 0.2397, the number of travel turns varies between 1.6227 and 1.9071, and the total number of turns per pass varies between 3.5373 and 3.8171.

TABLE 1. Schedule of Turn Values for Ellipse with a = 220 *mm*, e = 0.5

	Start-to-Far			Far-to-Start			
P	Pause	BC	Travel	Pause	BC	Travel	Total
0	0.0000	0	1.8165	0.0093	3	1.8634	3.6892
1	0.0305	6	1.6348	0.0122	9	1.9071	3.5847
2	0.0125	12	1.6504	0.0632	0	1.8165	3.5427
3	0.0093	3	1.8634	0.0305	6	1.6348	3.5380
4	0.0122	9	1.9071	0.0125	12	1.6504	3.5823
5	0.2397	14	1.6646	0.0101	2	1.9026	3.8171
6	0.0157	5	1.6249	0.0294	8	1.8800	3.5500
7	0.0098	11	1.8111	0.0518	14	1.6646	3.5373
8	0.0101	2	1.9026	0.0157	5	1.6249	3.5533
9	0.0294	8	1.8800	0.0098	11	1.8111	3.7303
10	0.1237	13	1.6227	0.0168	1	1.9022	3.6653
11	0.0107	4	1.7255	0.0786	7	1.7239	3.5386
12	0.0094	10	1.8897	0.0206	13	1.6227	3.5424
13	0.0168	1	1.9022	0.0107	4	1.7255	3.6551
14	0.0786	7	1.7239	0.0094	10	1.8897	3.7016

FIGURE 5. Comparison of Delivery Point Trajectories for Three Different Half-Passes

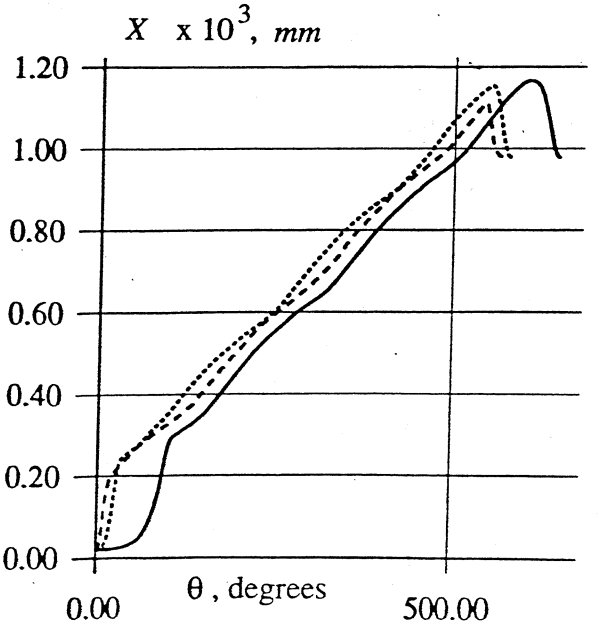

Figure 5 shows the delivery point trajectories for the first three start-to-far-end half-passes as a function of the mandrel rotation θ in degrees. The initial θ-value is referenced to 0 degrees in each case for purposes of comparison. As can be seen, although the winding point trajectory on the mandrel surface remains the same, the delivery point trajectory depends strongly upon the initial contact point for on the mandrel perimeter for each pass.

2.2 Polygonal Shapes

2.2.1 Geometry

Figure 6 [11] shows a pentagonal mandrel cross-section in order to illustrate the polygonal case. The following steps define the winding geometry:

1. The cross-section is divided into triangles by joining the vertices to the axis of rotation O (see Fig. 6).
2. The parameters r_k, s_k, α_k, and β_k shown in Fig. 6 are specified or calculated. For example, the r_k and α_k may be specified to define the polygon, and the s_k and β_k may then be calculated from the law of cosines.
3. The distance, d, of the delivery point D from the axis of rotation O, and the angle, λ, of elevation of D from the fixed horizontal axis X are specified.

FIGURE 6. Polygonal Mandrel Geometry

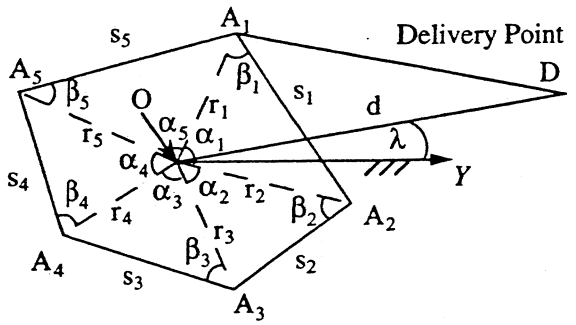

4. For each side s_k, the fiber length f_k from vertex A_k to the delivery point D at the instant when the fiber just covers side s_k (segment A_kA_{k+1}) is calculated. At these instants, triangle OA_kD has the included angle $\angle OA_kD = \beta_k$, as shown in Fig. 7 for side 1. The including sides A_kO and A_kD have lengths r_k and f_k, respectively. By application of the law of cosines, f_k may be written as

$$f_k = r_k\cos\beta_k + \sqrt{(r_k\cos\beta_k)^2 + d^2 - r_k^2} \quad \text{(EQ 31)}$$

The length $A_{k+1}D$ is analogous to the fiber length l defined for smooth shapes, and is given by

$$l_k \equiv A_{k+1}D = f_k - s_k \quad \text{(EQ 32)}$$

5. For the same situation considered in step 4 above, the angles γ_k included by sides OA_k and OD of the triangles OA_kD are found. These sides have lengths r_k and d, respectively, so that application of the law of cosines yelds

$$\cos\gamma_k = \frac{r_k^2 + d^2 - f_k^2}{2r_k d} \quad \text{(EQ 33)}$$

6. For each side s_k, find θ_k, the position of the inscribed axis y with respect to the fixed axis Y for which the fiber just covers s_k. Fig. 7 [11] shows this situation for side 1, with the inscribed, rotating axis y coinciding with r_1. The angles θ_k are found as follows:

$$\theta_1 = \gamma_1 + \lambda \quad \text{(EQ 34)}$$

$$\theta_k = \gamma_k + \sum_{j=1}^{k-1}\alpha_j + \lambda \quad \text{(EQ 35)}$$

for $k = 2$ to n, where n is the number of sides of the polygon.

FIGURE 7. Position at Which Fiber Just Covers Side 1.

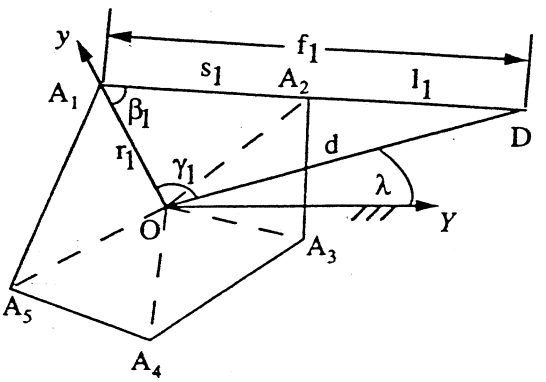

2.2.2 Equation of Motion

For polygonal shapes, knowledge of $X(t)$ at certain discrete times determines the laydown pattern, since filament is only laid down at those instants when the filament band just covers one of the sides of the polygon.

The longitudinal position of the laydown point x is found for an arbitrary filament support trajectory X as follows

$$x_i = x_{i-1} + \left(\frac{X_i - x_i}{l_{i'}}\right) s_{i'} \qquad \text{(EQ 36)}$$

where i is the iteration step, $i = 1, 2, \ldots$ and $i' = (k_0 + i - 1) \bmod n$, where n is the number of polygon sides and k_0 is the index of the initial side on which filament is laid. The index i' wraps around each time another full revolution of the mandrel is performed, i.e., each time i equals a multiple of n. The X_i are the delivery point positions at those mandrel positions $\theta_{i'}$ for which the fiber just covers sides $s_{i'}$. Equation (36) is directly analogous to (9), of which it is simply a discretized version, with the side length $s_{i'}$ corresponding to the differential arc length ds.

2.2.3 Winding-Angle Control

Winding-angle control for polygonal shapes is analogous to that for smooth shapes. This is not surprising, because (14) and (15) are based on a polygonal approximation of a smooth surface. These equations also apply to the polygonal case

$$x_i = x_{i-1} + s_{i'} \tan(\theta_f)_{i'} \qquad \text{(EQ 37)}$$

$$X_i = x_i + l_{i'} \tan(\theta_f)_{i'} \qquad \text{(EQ 38)}$$

with two changes:

1. The arc length approximation $\Delta s_{i-1,i}$ has been replaced by the side length $s_{i'}$.
2. The subscripts imply evaluation at the $\theta_{i'}$ for which the fiber just covers sides $s_{i'}$, rather than at the ϕ_i, which are not defined for the polygonal case.

As in (36), $i' = (k_0 + i - 1) \bmod n$, where n is the number of polygon sides and k_0 is the initial side on which filament is laid. The result is a set of discrete pairs $(X_i, \theta_{i'})$ giving the relationship between the mandrel rotation angle θ and the filament support position X in order to achieve a desired winding angle.

2.2.4 Surface-Coverage Algorithm

For polygonal shapes, as for smooth shapes, there are three basic steps for achieving closure. The number of bands and the band-center positions are calculated in a similar way. In addition to calculating pause values, the final step consists of adjusting the initial and final winding angles in each half-pass. Each of these steps is described below.

Number of Bands m. The number of bands is calculated as for smooth shapes, except that the perimeter is

$$P = \sum_{i=1}^{n} s_i \qquad \text{(EQ 39)}$$

i.e., the sum of the side lengths, where n is the number of sides.

Band-Center Positions BC_i. The band-center positions measured along the perimeter are

$$BC_i = \frac{i \times P}{m} \qquad \text{(EQ 40)}$$

for $i = 0, 1, \ldots, m - 1$.

FIGURE 8. Example of Endpoint Winding-Angle Adjustments for Polygonal Shapes

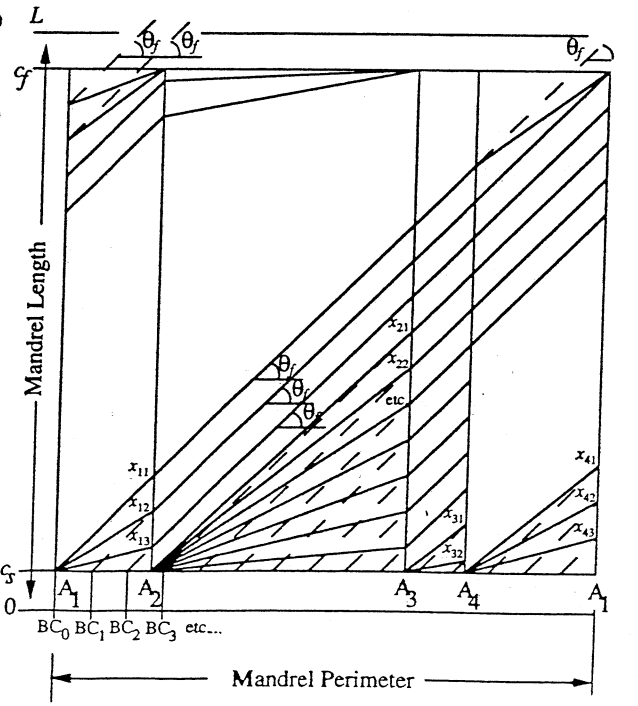

Pause Values and Endpoint Winding-Angle Adjustments. For smooth shapes, band centers can be laid down at any desired position along the perimeter of the mandrel end, since the band contact point shifts continuously. For polygonal shapes, band centers can only be laid down at the discrete points corresponding to the vertices of the polygon. This is illustrated in Figure 8, where a four-sided polygonal mandrel is unfolded to lie flat, and the vertices A_k and their projections along the mandrel length are indicated. A given band segment starts at vertex A_k and ends at vertex A_{k+1}, with a constant winding angle in between. As a result, a single vertex at the mandrel end must generally be the departure point for multiple bands. In order to align the bands for closure, the band segments originating from a given vertex are laid down in a fan pattern, having varying winding angles.

The following steps are performed to achieve closure:

1. For each vertex A_k, find the index m_k of the first band center position originating from that vertex. This is the first band center whose distance along the perimeter is greater than or equal to the distance of the vertex along the perimeter. The position of the initial band center BC_0 is arbitrarily chosen to correspond to the vertex A_1, so that $m_1 = 0$. To find the remaining m_k, for each vertex A_k, $k = 2, ..., n$, increment i starting with $i = m_{k-1} + 1$ until

$$BC_i \geq p_k \equiv \sum_{j=1}^{k-1} s_j \qquad \text{(EQ 41)}$$

where p_k is the perimeter position of the k^{th} vertex measured with respect to vertex A_1. Set m_k equal to the resulting value of i.

2. For each of the bands originating at the k^{th} vertex, find the longitudinal position x of the band at the $k{+}1^{st}$ vertex. Do this for each of the n vertices. As shown in Fig. 8, the x_{kb} are found by extending segments from the band-center positions on side s_k with desired winding angle θ_f until they intersect the border with the next side, s_{k+1}. Once the bands originating at vertex k have reached these points, they are correctly positioned to continue with the desired winding angle. For the k^{th} vertex, the position of the initial band is

$$x_{k1} = x_s + (p_{k+1} - BC_{m_k}) \tan\theta_f \qquad \text{(EQ 42)}$$

where x_s is the initial longitudinal position at the start end (typically w, half the band width). The remaining bands are spaced at intervals of a band width, B, from the initial

$$x_{kb} = x_{k1} - B(b-1) \qquad \text{(EQ 43)}$$

where $b = 1, 2, ..., (m_{k+1} - m_k)$, x_{kb} is the longitudinal position at the $k{+}1^{st}$ vertex of the b^{th} band originating at the k^{th} vertex, and $(m_{k+1} - m_k)$ is the number of bands originating there.

3. Identify the start-end arrival vertex as k_{sa}. Pause at the start end until the first vertex with empty positions corresponding to the x_{kb} found in step 2 is reached. This is the start-end departure vertex k_{sd}. The start-end pause value is $\theta_{sp} = \theta_{k_{sd}} - \theta_{k_{sa}}$.
4. At vertex k_{sd}, choose the next open $x_{k_{sd}b}$ to occupy. This may be done in any order at a given vertex, but sequential order is simplest from a bookkeeping standpoint. For the start-to-far-end half-pass, the initial longitudinal position x_0 is x_s, x_1 is given by the chosen $x_{k_{sd}b}$, and

$$S_1 = c_1 + l_{k_{sd}}\left(\frac{c_1}{s_{k_{sd}}}\right) \qquad \text{(EQ 44)}$$

5. Use (37)-(38) to calculate the x_i and X_i for the start-to-far-end half-pass. This results in a set of $(\theta_{i'}, X_i)$ pairs. As illustrated in Figure 8, the final side laid down in a given half-pass will not generally have winding angle θ_f. For that (final) i_f for which the value for x calculated in (37) is greater than or equal to x_f, the far-end value of x (typically the mandrel length L minus half the band width B), calculate X as follows

$$X_{i_f} = x_f + l_{i'_f}\left(\frac{x_f - x_{i_f-1}}{s_{i'_f}}\right) \qquad \text{(EQ 45)}$$

Since the side $s_{i'_f}$ will now have been laid down, this places the filament at the far-end arrival vertex $k_{fa} = i'_f + 1$.

6. Pause at the far end until the first vertex with empty positions corresponding to the x_{kb} found in step 2 is reached. This is the far-end departure vertex k_{fd}. The far-end pause value is $\theta_{fp} = \theta_{k_{fd}} - \theta_{k_{fa}}$.

7. At vertex k_{fd}, choose the next open $x_{k_{fd}b}$ to occupy. For the far-to-start-end half-pass, the initial longitudinal position x_0 is x_f, x_1 is given by $L - x_{k_{fd}b}$, and

$$X_1 = x_1 - l_{k_{fd}}\left(\frac{L - x_1}{s_{k_{fd}}}\right) \qquad \text{(EQ 46)}$$

8. As in step 5, use (37)-(38) to calculate the x_i and X_i for the far-to-start-end half-pass. Precede, however, the second term of each equation with a negative sign, since $(\theta_f)_{far\text{-}to\text{-}start} = -(\theta_f)_{start\text{-}to\text{-}far}$. For that i_f for which x is less than or equal to x_s, calculate X as follows

$$X_{i_f} = x_s - l_{i'_f}\left(\frac{x_{i_f - 1} - x_s}{s_{i'_f}}\right) \qquad \text{(EQ 47)}$$

This places the filament at the start-end arrival vertex for the next pass $k_{sa} = i'_f + 1$.

9. Perform steps 3 through 8 a total of m times, using the vertex k_{sa} found in step 8 as the new start-end arrival vertex in step 3. Once all m positions x_{kb} have been laid down at both ends, the layer is complete.

2.2.5 Surface-Coverage Example

A four-sided polygon is used to illustrate the calculations involved in the polygonal case. The radii r_k and internal angles α_k are arbitrarily specified as r_{1-4}= 200, 220, 240, 260 *mm* and α_{1-4} = 100°, 80°, 60°, 120°. The side lengths s_k and included angles β_k are then determined from the law of cosines as s_{1-4} = 322, 296, 251, 400 *mm* and β_{1-4} = 42.3°, 53.0°, 64.0°, 25.7°. Arbitrarily choosing a minimum standoff of 100 *mm* results in a distance *d* from the mandrel axis of rotation of 360 *mm*. The angle of elevation λ is set to 0°.

Using (31)-(35) to determine the remaining parameters, the following table of values can be constructed, where lengths are given in *mm*, angles in degrees.

TABLE 2. Geometric Parameters for Polygonal Example

Index	*r*	*s*	*α*	*β*	*f*	*l*	*γ*	*θ*
1	200	322	100	42.3	482	160	115.8	115.8
2	220	296	80	53.0	447	151	97.8	197.8
3	240	251	60	64.0	394	143	79.2	259.2
4	260	400	120	25.7	576	177	136.1	376.1

The polygonal closure algorithm is now applied. The perimeter P is found to be 1268 *mm* by summing the side lengths. For a desired winding angle θ_f = 30° and band width B = 39.5 *mm*, (20) yields m = 18.53. Rounding m down to 18, we obtain an adjusted winding angle θ_f = 29.3°. Setting p = 0 at vertex A_1, the band-center positions are at intervals of P/m = 70.45 *mm*, as follows: {0, 70.5, 140.9, 211.4, 281.8, 352.3, 422.7, 493.2, 563.6, 634.1, 704.5, 775.0, 845.5, 915.9, 986.4, 1056.8, 1127.3, 1197.7} *mm*. The indices m_k corresponding to the first band-center positions on each of the k sides are m_1 = 0, m_2 = 5, m_3 = 9, and m_4 = 13. The intercepts c_{kb} are c_{11-15} = 200, 161, 121, 82, 42 *mm*, c_{21-24} = 169, 129, 90, 50 *mm*, c_{31-34} = 151, 112, 72, 33 *mm*, c_{41-45} = 217, 178, 138, 99, 59 *mm*.

Figure 9 illustrates a partial result of the polygonal closure algorithm for the current example, where the mandrel has begun in the θ = 0° position. All five filament delivery point trajectories originating at vertex 1 for the start-to-far-end traversal of the mandrel are shown. The exact position of the filament support at mandrel rotation values between those for which a side is laid down is irrelevant. Markers indicate the crucial points which must be attained in each trajectory.

FIGURE 9. Delivery Point Trajectories Originating at Vertex 1 for a Four-Sided Polygon Example

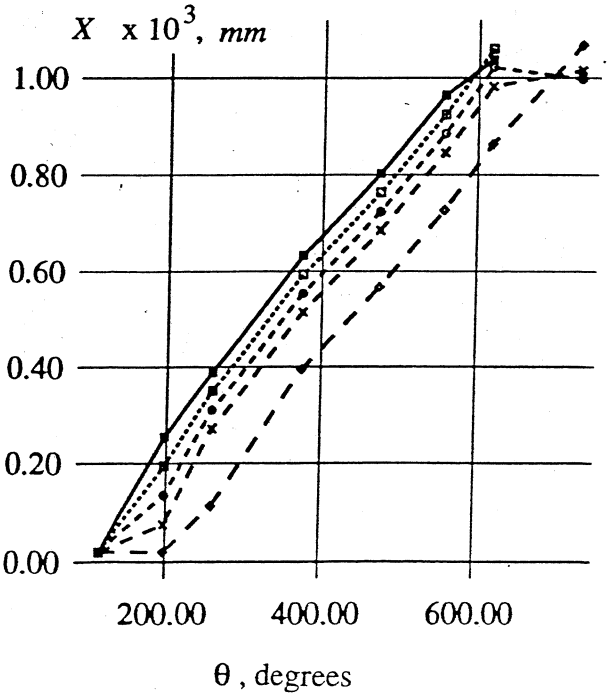

3.0 SUMMARY AND CONCLUSION

The work described here extends the computationally efficient "geometric" winding-angle control algorithms for cylindrical non-axisymmetric smooth and polygonal mandrel shapes presented in [10, 11] in two ways. First, a method for varying, rather than constant, winding-angle control is introduced. Second, closure algorithms are added to the winding-angle control algorithms in order to achieve surface coverage of the wound parts. The relationship between the discrete, "geometric" approach presented by Mazumdar and Hoa and the continuous differential equation of winding was demonstrated. Finally, the analogy between the smooth- and polygonal-shape winding algorithms, both of which use polygonal approximations of the mandrel profile, was elucidated. The method of winding-angle control and surface coverage presented here can be straightforwardly implemented on any two-axis computer-controlled winding-machine.

References

1. C.D. Hermansen and R.R. Roser, 36th Annual Conference, Reinforced Plastics/Composites Institute, The Society of the Plastics Industry, Inc., Paper 5-A, (1981).
2. C. Barbalat, P. Denizet, and T. Massard, 30th International SAMPE Symposium, pp. 1265-1274, (1985).
3. H. Hamouda, T.J. Kang, and A. El-Shiekh, 34th International SAMPE Symposium, pp. 1130-1142, (1989).
4. K.-W. Kirberg, G. Menges, and J. Mitscherling, 42nd Annual Conference, Reinforced Plastics/Composites Institute, The Society of the Plastics Industry, Inc., Paper 6-F, (1987).
5. D.G. Elliman, et.al., Advanced Manufacturing Engineering, 1, pp. 15-20, (1988).
6. G. Menges and M. Effing, 43nd Annual Conference, Reinforced Plastics/Composites Institute, The Society of the Plastics Industry, Inc., Paper 20-D, (1988).
7. W. Michaeli and M. Goedel, Pressure Vessels and Piping Conference, Nashville, Tennessee, pp. 35-40, (1990).
8. W. Michaeli, et.al., Kunststoffe, 81, (10), pp. 56-58, (1991).
9. R.E. Allard, et.al., 41st Annual Conference, Reinforced Plastics/Composites Institute, The Society of the Plastic Industry, Inc., Paper 3-A, (1986).
10. S.K. Mazumdar and S.V. Hoa, Composites Manufacturing, 2, (1), pp. 23-30, (1991).
11. S.K. Mazumdar and S.V. Hoa, Composites Manufacturing, 2, (1), pp. 31-38, (1991).
12. A.P. Minakov, Tekst. Prom. (USSR), (10), pp. 10-18, (1944).